Bioactive Materials 5 (2020) 680–693

Contents lists available at ScienceDirect

Bioactive Materials

journal homepage: http://www.keaipublishing.com/biomat

Biofunctional magnesium coated Ti6Al4V scaffold enhances osteogenesis and angiogenesis *in vitro* and *in vivo* for orthopedic application

Peng Gao[a,b], Bo Fan[a], Xiaoming Yu[c,d], Wenwen Liu[a], Jie Wu[a], Lei Shi[a], Di Yang[a], Lili Tan[c], Peng Wan[c], Yulin Hao[c], Shujun Li[c], Wentao Hou[c], Ke Yang[c,**], Xiaokang Li[a,***], Zheng Guo[a,*]

[a] Department of Orthopedics, Xijing Hospital, Fourth Military Medical University, Xi'an, 710032, China
[b] Department of Joint Surgery and Sports Medicine, Hunan Provincial People's Hospital and The First Affiliated Hospital of Hunan Normal University, Changsha, 410016, PR China
[c] Institute of Metal Research, Chinese Academy of Science, Shenyang, 110016, China
[d] School of Material Science and Engineering, Shenyang Ligong University, Shenyang, 110159, China

ARTICLE INFO

Keywords:
Porous Ti6Al4V scafflod
Surface modification
Magnesium coating
Osteogenesis
Angiogenesis

ABSTRACT

The insufficient osteogenesis and osseointegration of porous titanium based scaffold limit its further application. Early angiogenesis is important for scaffold survival. It is necessary to develop a multifunctional surface on titanium scaffold with both osteogenic and angiogenic properties. In this study, a biofunctional magnesium coating is deposited on porous Ti6Al4V scaffold. For osseointegration and osteogenesis analysis, *in vitro* studies reveal that magnesium-coated Ti6Al4V co-culture with MC3T3-E1 cells can improve cell proliferation, adhesion, extracellular matrix (ECM) mineralization and ALP activity compared with bare Ti6Al4V cocultivation. Additionally, MC3T3-E1 cells cultured with magnesium-coated Ti6Al4V show significantly higher osteogenesis-related genes expression. *In vivo* studies including fluorochrome labeling, micro-computerized tomography and histological examination of magnesium-coated Ti6Al4V scaffold reveal that new bone regeneration is significantly increased in rabbits after implantation. For angiogenesis studies, magnesium-coated Ti6Al4V improve HUVECs proliferation, adhesion, tube formation, wound-healing and Transwell abilities. HUVECs cultured with magnesium-coated Ti6Al4V display significantly higher angiogenesis-related genes (HIF-1α and VEGF) expression. Microangiography analysis reveal that magnesium-coated Ti6Al4V scaffold can significantly enhance the blood vessel formation. This study enlarges the application scope of magnesium and provides an optional choice to the conventional porous Ti6Al4V scaffold with enhanced osteogenesis and angiogenesis for further orthopedic applications.

1. Introduction

Disadvantages of bone autografts and allografts such as donor-site complications, supply shortage and disease transmission potentiality have prompted the exploration of artificial bone substitutes [1,2]. Porous titanium scaffolds manufactured through 3D printing technology with reduced stress shielding, completely interpenetrated and adjustable pores which have similar mechanical properties with nature bone are thus promising for bone defect reconstruction [3–5]. Nevertheless, an insufficient rate of osteoconduction and integration of porous titanium scaffold could affect long-term survival, which limits its further application [6,7]. Therefore, a surface modification approach aiming to enhance the bioactivity and function of porous titanium scaffold has been introduced [8]. A wide variety of surface modification approaches for titanium and titanium alloys in the biomedical field have been introduced. Based on the methods of surface treatments, surface modification approaches can be classified into mechanical, chemical, and physical methods [9,10]. Such as machining, grinding, acid etching, sol-gel, electrophoretic deposition, alkali etching, anodization, micro-arc oxidation (MAO), and multi-arc ion plating [11–17]. These approaches focused on the modification of the titanium and titanium alloys surface topography, morphology, and additional coating.

However, vast majority of the surface modification approaches only focus on osseointegration and osteogenesis of the porous titanium

Peer review under responsibility of KeAi Communications Co., Ltd.
* Corresponding author.
** Corresponding author.
*** Corresponding author.
E-mail addresses: kyang@imr.ac.cn (K. Yang), lxkfmmu@163.com (X. Li), guozheng@fmmu.edu.cn (Z. Guo).

https://doi.org/10.1016/j.bioactmat.2020.04.019
Received 19 March 2020; Received in revised form 27 April 2020; Accepted 28 April 2020

Table 1
Primers used in Real-Time PCR.

Target gene	Forward primer (5′-3′)	Reverse primer (5′-3′)
ALP	TTGGGCAGGCAAGACACA	GAAGGGAAGGGATGGAGGAG
Col-1	GACATGTTCAGCTTTGTGGACCTC	GGGACCCTTAGGCCATTGTGTA
OCN	ACCATCTTTCTGCTCACTCTGCT	CCTTATTGCCCTCCTGCTTG
Runx2	GAACCAAGAAGGCACAGACAGA	GGCGGGACACCTACTCTCATAC
OPN	TACGACCATGAGATTGGCAGTGA	TATAGGATCTGGGTGCAGGCTGTAA
VEGF	GAGGAGCAGTTACGGTCTGTG	TCCTTTCCTTAGCTGACACTTGT
HIF1α	GAACGTCGAAAAGAAAAGTCTCG	CCTTATCAAGATGCGAACTCACA
GAPDH	TGCTGGTGCTGAGTATGTGGT	AGTCTTCTGGGTGGCAGTGAT

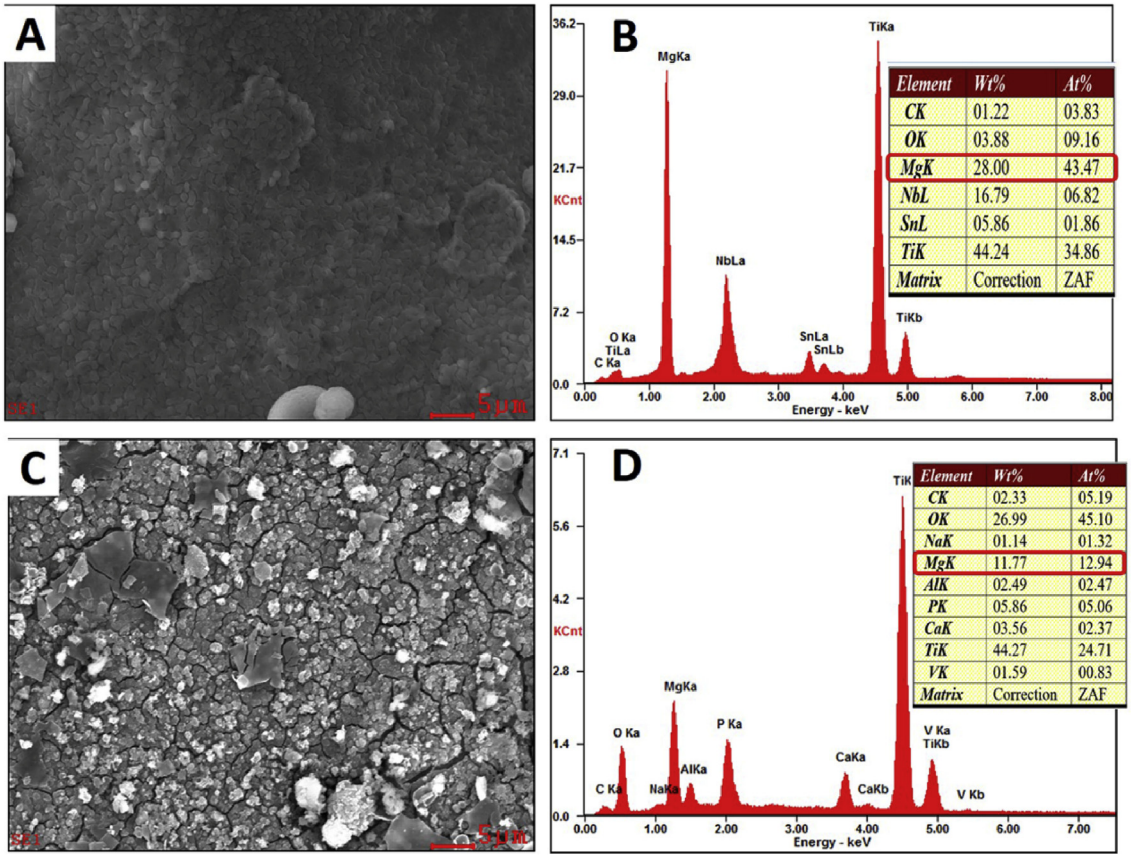

Fig. 1. SEM images and energy spectrum analysis of Mg-coated Ti6Al4V scaffold before (A, B) and after (C, D) immersion.

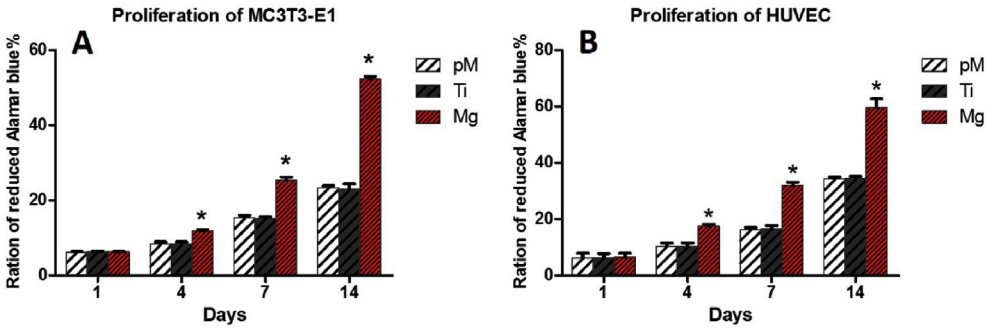

Fig. 2. Measurement of MC3T3-E1 cell proliferation by alamarBlue colorimetric assay after 1, 4, 7 and 14 days of cultivation. Asterisks (*) indicate statistical significance compared with the Ti and pM groups, $p < 0.05$. Pure complete medium (pM); Ti6Al4V sample extraction (Ti); Mg-coated Ti6Al4V sample extraction (Mg) (n = 3 for each group).

scaffolds [18,19]. There is a lack of emphasis on angiogenesis of the porous titanium scaffolds which is a crucial factor for scaffold favorable long-term fixation, as abundant blood vessels are indispensable to favorable osteoblast function and rapid generation of new bone [20,21]. Osteogenic cells growing into the scaffold require abundant blood and oxygen supply for direct osteogenesis [22]. The early new blood vessels formed by vascular endothelial cells in peri-implant bone tissue are vital for rapid osseointegration and osteogenesis which increase the success rate of scaffold implantation [23]. Consequently, a biofunctional coating with both osteogenesis and angiogenesis properties is required for long term fixation and survival of porous titanium scaffold.

Recently, growing literatures have shown that biodegradable Mg-

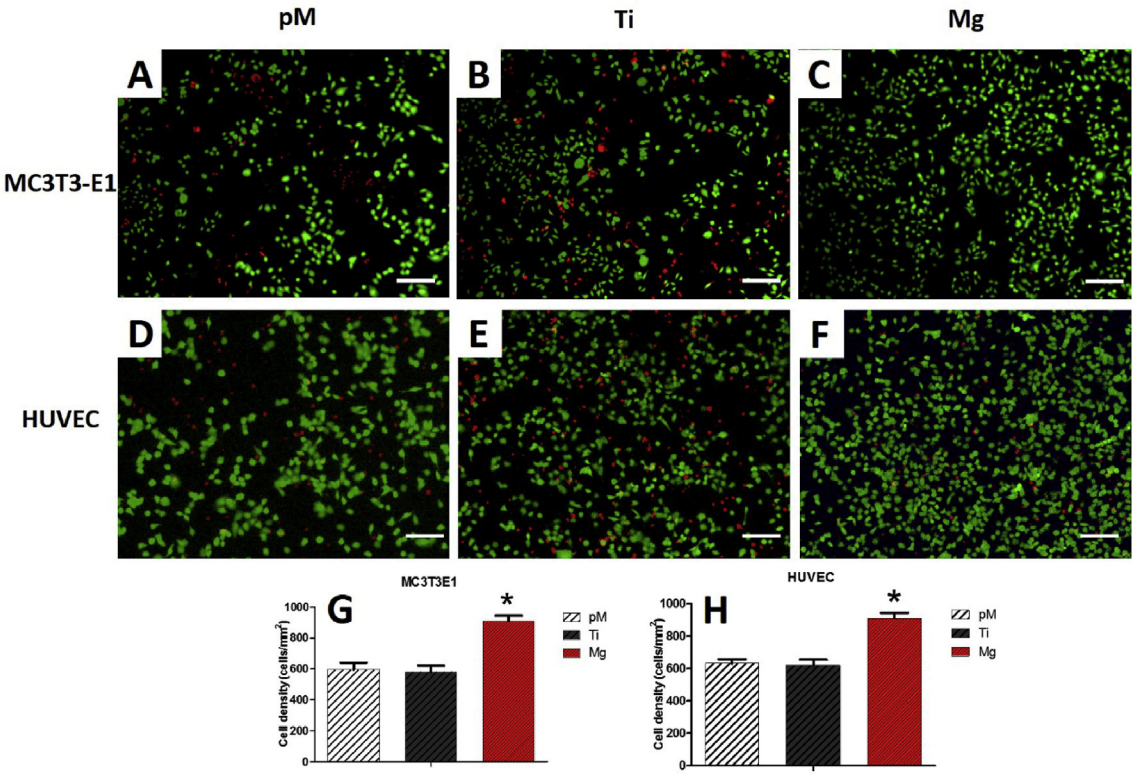

Fig. 3. Proliferation and viability of MC3T3-E1 cells (A, B, C) and HUVECs (D, E, F) by Calcein-AM/PI double stain afer one week cultivation. Quantitative analysis (G, H) demonstrated that high cell density was maintained in Mg group. Asterisks (*) indicate statistical significance compared with the Ti and pM groups, $p < 0.05$. Pure complete medium (pM); Ti6Al4V sample extraction (Ti); Mg-coated Ti6Al4V sample extraction (Mg) (n = 3 for each group, Scale bar = 100 μm).

based alloys are becoming revolutionary candidates for biomedical implants. Mg is an essential element that has a crucial role in normal bone metabolism [24,25]. Mg-based alloys have promising osteogenic effects during bone fracture healing and bone defect reconstruction [26,27]. Early adhesion of osteoblastic cells around the bone substitute surfaces is essential for new bone formation [28–30]. After implantation, Mg reacts with body fluid and then corrodes, releasing Mg ions which are known to enhance cellular adhesion [31–33]. Therefore, Mg can be used in implants with the intention of utilizing its cellular adhesion enhancement effect to facilitate new bone formation [34]. In addition to osteogenic activity, Mg has also been found to play a role in formation of new blood vessels, but the relevant mechanism has not yet been fully studied [35,36]. Nevertheless, superfluous hydrogen, high pH and insufficient biomechanical support caused by rapid and irregular degradation of Mg may cause gas-filled cavities which lead to implant failure [37]. A high pH would be detrimental to cells if the corrosion rate of Mg surpass the buffering ability of the surrounding tissue [38]. The rapid degradation and insufficient biomechanical support limit the application of Mg-based alloy which are mainly used as screw and plate in non-load bearing position. An extension of Mg application is necessary due to its favorable bioactivity.

To improve osseointegration, osteogenesis, and angiogenesis for long-term scaffold survival, it is necessary to develop a multifunctional surface of porous titanium scaffold with both osteogenic and angiogenic properties. To combine the advantages and avoid the disadvantages of porous titanium scaffold and Mg, a biofunctional Mg coating was successfully added to a titanium alloy (Ti6Al4V) scaffold, with an expectation of enlarging the use of Mg in orthopedic application and possessing sufficient biomechanical support, osseointegration, osteogenesis, and angiogenesis functions for orthopedic application. The biofunctional Mg coating was preliminarily proven to promote osteointegration and have no evident side effects related to Mg corrosion in our previous study [17]. Nevertheless, the early angiogenesis effects *in vitro* and *in vivo* as well as long-term bone formation effects of Mg-coated Ti6Al4V scaffold are still unknown. In this work, MC3T3-E1 cells (preosteoblast cells) and HUVECs were used to study the *in vitro* osteogenesis and angiogenesis effects of Mg-coated Ti6Al4V scaffold, respectively. The early angiogenesis and long-term bone formation effects of Mg-coated Ti6Al4V scaffold *in vivo* were further evaluated with a rabbit model of femoral condylar defect.

2. Experimental section

2.1. The preparation of porous Ti6Al4V scaffolds and Mg coating

An electron beam melting system was applied to fabricate the porous Ti6Al4V scaffolds as mentioned previously [39]. Briefly, the STL data of a 3D model was transferred to the electron beam melting machine. ~30 μm Ti6Al4V powders were preheated to 650 °C to generate a cross-section layer with the electron beam scanning under a vacuum condition (~10^{-4} to 10^{-5} mbar). The process was repeated layer by layer until completion. The fabricated Ti6Al4V scaffold was 68 ± 5% in porosity with pore size of 710 ± 42 μm. The Mg coating deposition on Ti6Al4V scaffolds was performed as described previously [17]. Briefly, a high-purity Mg (99.99%) was applied to bombard and sputter the substrate surface. The constant target arc current used in the process was 50 A, and under $P_{Ar} = 3.5 \times 10^{-2}$ Pa for 5 min. The negative bias voltage application used a 0.12–0.16 A current density. During deposition, the distance between Ti6Al4V samples and the cathode arc target was 400 mm, and the total deposition time was 60 min. The substrate temperature T_s was set to 245 °C. All the samples used in this work were sterilized by Co^{60} radiation and sealed before experiments.

2.2. Preparation of extractions of Ti6Al4V with and without Mg coating

According to the ISO 10993-12 standard, sterilized and sealed disk-

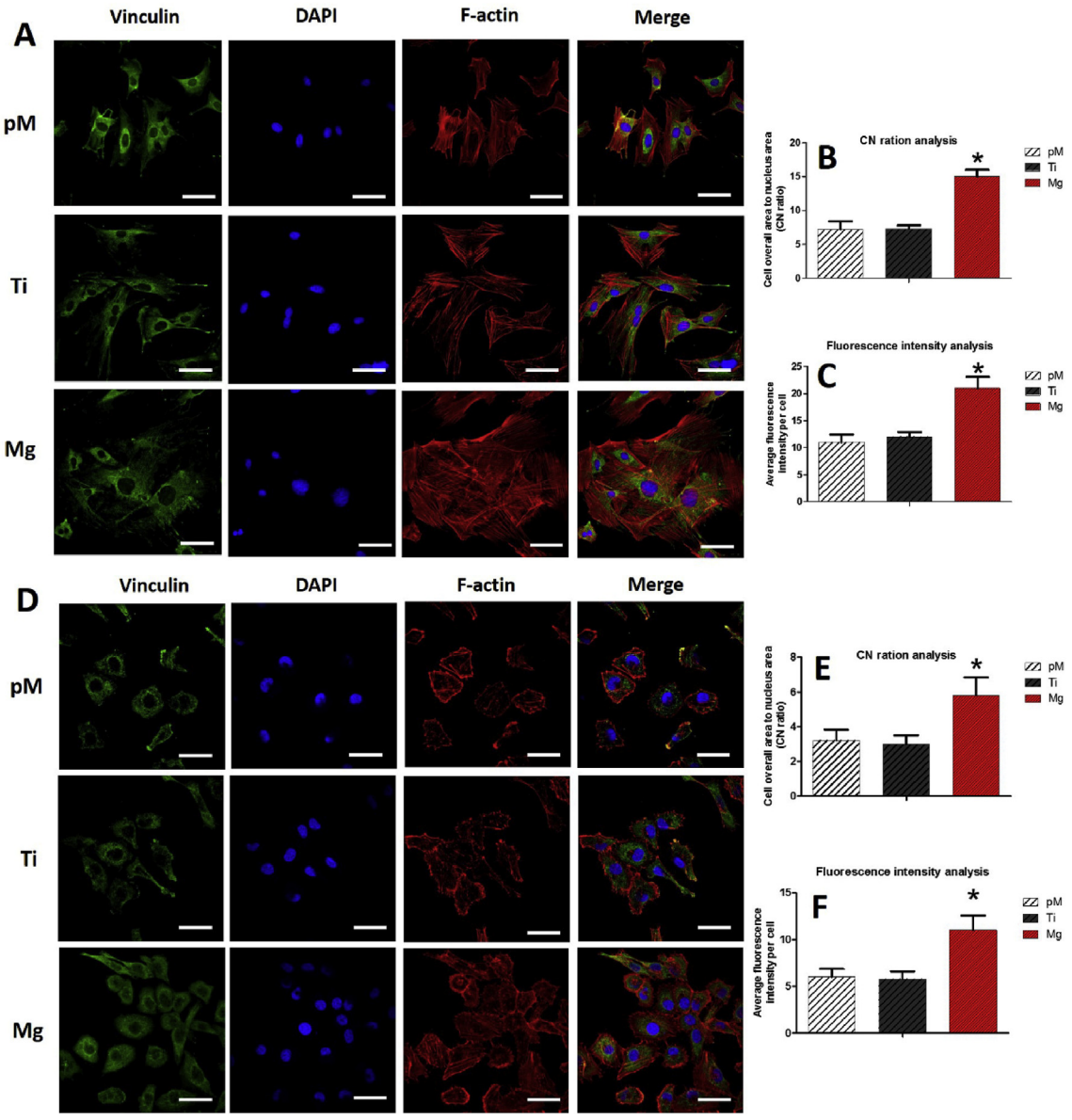

Fig. 4. Analyses of MC3T3-E1 (A) and HUVEC (D) cell adhesion with different extraction after incubation for 48 h by fluorescent detection. B, E show morphology analysis, and C, F show the fluorescence intensity of vinculin staining with different extraction, respectively. Three different fields were measured per sample. Asterisks (*) indicate statistical significance compared with the Ti and pM groups, $p < 0.05$. Pure complete medium (pM); Ti6Al4V sample extraction (Ti); Mg-coated Ti6Al4V sample extraction (Mg) (n = 3 for each group, scale bar = 50 μm).

shaped Ti6Al4V samples with and without Mg coating were immersed in complete α-MEM (for MC3T3-E1 cell culture) and F–12K medium (for HUVECs culture). Immersions were carried out in medium with a 50 mL/cm^2 of volume-to-surface area [40]. All immersions were placed in a humidified thermostatic cell incubator for 48 h (37 °C, 5% CO_2). Both Mg-coated Ti6Al4V scaffold extraction (Mg) and bare Ti6Al4V scaffold sample extraction (Ti) were collected under sterile conditions and placed in a 4 °C refrigerator for later use. Pure complete medium (pM) was used as a control. The Mg coating surface morphology was examined with X-ray diffraction and scanning electron microscopy (SEM).

2.3. In vitro studies

2.3.1. Cell culture

Complete α-MEM and F–12K medium were used to culture MC3T3-E1 cells and HUVECs respectively. All cells were incubated in a humidified incubator (37 °C, 5% CO_2). Medium was changed with fresh complete medium every 2 days.

2.3.2. Cell proliferation and viability

Cell proliferation and viability cultured using the Mg-coated Ti6Al4V scaffold extraction (Mg) and bare Ti6Al4V scaffold extraction (Ti), as well as pure complete medium (pM), were evaluated at 1, 4, 7, and 14 days, respectively, using an alamarBlue colorimetric assay (Invitrogen, Carlsbad, CA, USA). 3×10^3 (MC3T3-E1 cells) and 2×10^3 (HUVECs) cells per well were seeded on 96-well plates. Each well was added with 10 μL of 10% (v/v) alamarBlue solution and cultured for 3 h. A microplate reader was applied to test the absorbance of the culture medium at 570/600 nm in triplicate.

Following the manufacturer's guidance, cell viability was further assessed by the Calcein-AM/PI Double Stain Kit. MC3T3-E1 cells and HUVECs cultured with pM, Ti and Mg were resuspended and seeded on 24-well plates at a density of 5×10^3 and 4×10^3 cells per well, respectively. After 1-week cultivation, the cells were stained with calcein AM (acetoxymethyl) and PI (propidium iodide) for living and dead

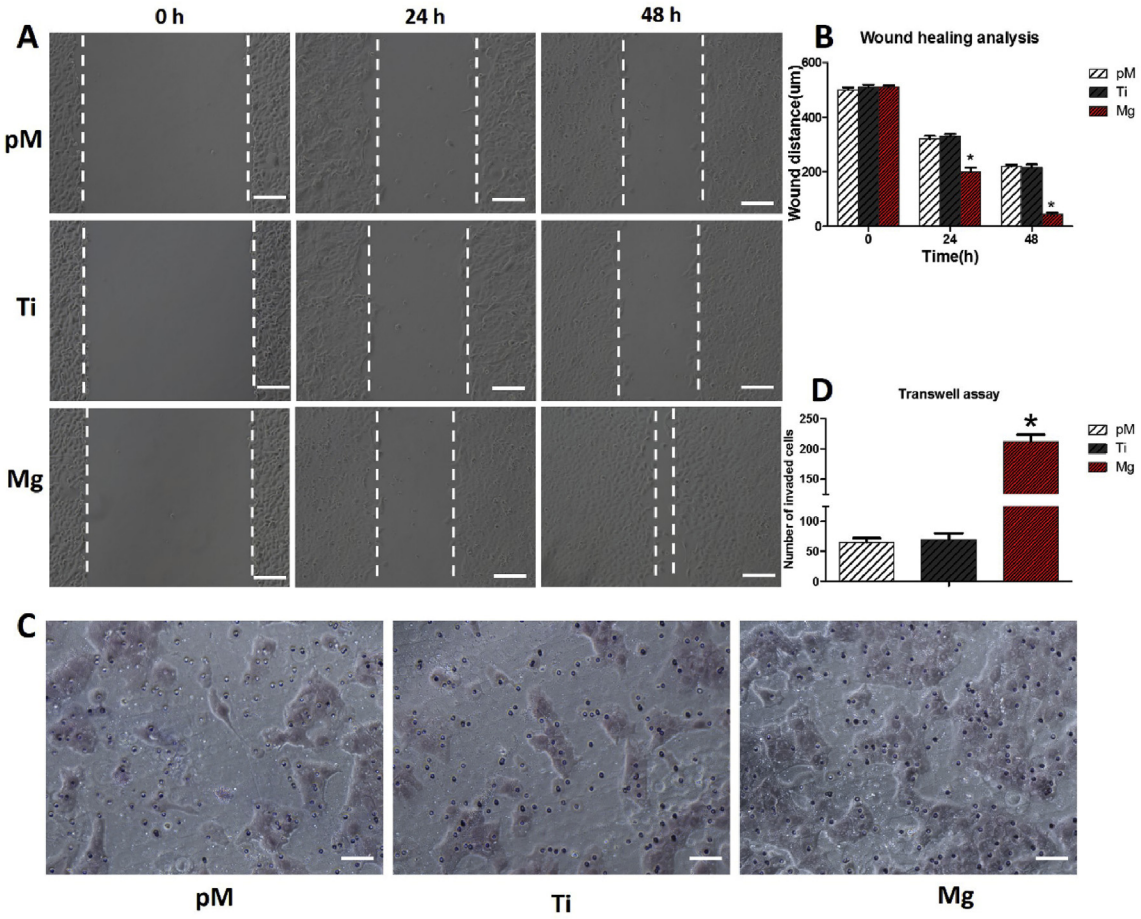

Fig. 5. Wound-healing assay and Transwell assay of HUVECs cultured with pM, Ti, and Mg extractions. (A) Representative migration images of HUVECs at different time points (0, 24, and 48 h) of different groups. (B) Quantitation of migration ability of different groups. (C) Transwell images of HUVECs cultured with pM, Ti, and Mg extraction. (D) Quantitations of invaded cells of different groups. Asterisks (*) indicate statistical significance compared with the Ti and pM groups, $p < 0.05$. Pure complete medium (pM); Ti6Al4V sample extraction (Ti); Mg-coated Ti6Al4V sample extraction (Mg) (n = 3 for each group, scale bar: A = 100 μm. C = 50 μm).

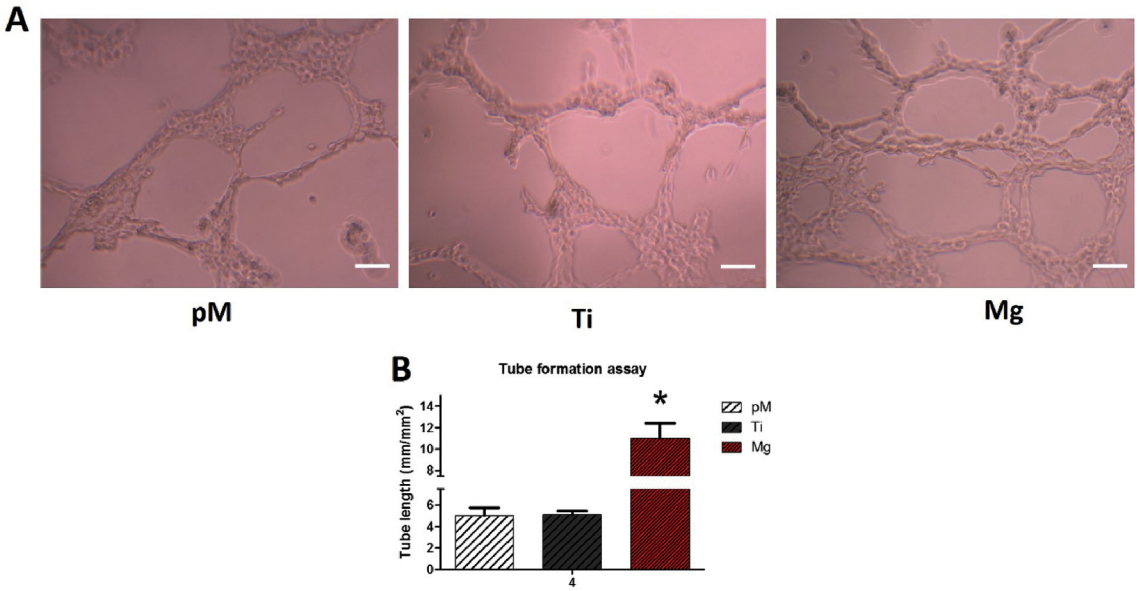

Fig. 6. Tube formation assay of HUVECs cultured with pM, Ti, and Mg extractions. (A) Representative tube formation images of HUVECs of different groups showing tube length; branch points were significantly higher in Mg group than in Ti and pM groups. (B) Quantitations of tube formation of different groups. Asterisks (*) indicate statistical significance compared with the Ti and pM groups, $p < 0.05$. Scale bar = 100 μm. Pure complete medium (pM); Ti6Al4V sample extraction (Ti); Mg-coated Ti6Al4V sample extraction (Mg) (n = 3 for each group).

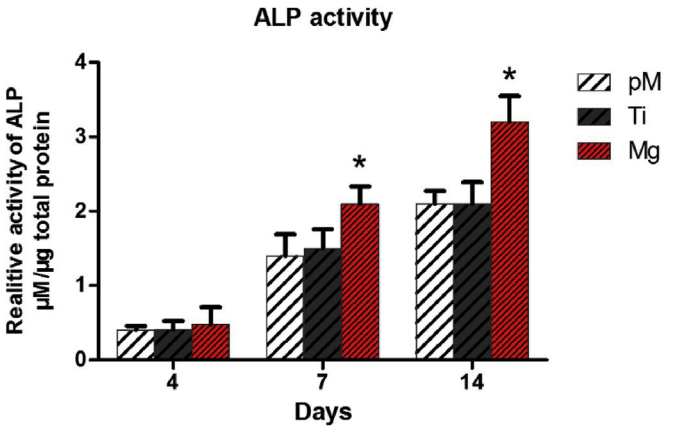

Fig. 7. Quantitative ALP activities of MC3T3-E1 cells cultured with pM, Ti, and Mg extraction. Asterisks (*) indicate statistical significance compared with the Ti and pM groups, $p < 0.05$. Pure complete medium (pM); Ti6Al4V sample extraction (Ti); Mg-coated Ti6Al4V sample extraction (Mg) (n = 3 for each group).

cells, respectively. Cells were imaged using 490 nm wavelength excitation for green living cells and 545 nm for red dead cells by a confocal laser scanning microscope.

2.3.3. Morphologies of cells

Vinculin and filamentous actin (F-actin) were detected to assess the cell morphology as mentioned previously [6]. In brief, after incubation with different extractions for 1 week, MC3T3-E1 cells and HUVECs were resuspended and seeded on 24-well plates (5×10^4 per well both). Cells were fixed and permeabilized for bovine serum albumin blocking after 48h of cultivation. Then primary vinculin antibody was added for overnight incubation before incubated with secondary antibody (1:500). Subsequently, rhodamine-phalloidin and DAPI treatments were applied to stain cells. The vinculin expression and overall cell area to nucleus area ration (CN ratio) were assessed with Image-Pro Plus 6.0.

2.3.4. Wound-healing assay and transwell assay of HUVECs

To test the motility and migration activities of HUVECs cultivated with pM, Ti and Mg, 5×10^5 cells were seeded onto each well of 6-well plates to do the wound-healing assay. After 100% confluence of cells was achieved, a straight line was scraped in the middle of each well. All cells were cultivated with serum-free F–12K medium and observed at 0, 24, and 48 h post scrape. Images were acquired of every well to monitor the cell migration process at each time point. The distance between two scratch edges (wound width) was calculated.

8.0-μm PET membranes BioCoat™ Matrigel® invasion chambers (Corning, NY, USA) were used to study cell invasion activity. In brief, 300 μL serum-free medium suspension containing 3×10^4 cells (starved-treated overnight) per well was added to the upper chamber, while 750 μL of antibiotic-free complete F–12K medium in the lower chamber. A cotton swab was used to scrub the remaining cells in the upper chamber after cultivation for 48 h. Cells migrated through the chamber membrane were fixed and washed, followed by hematoxylin staining for 15 min. The invaded cells were counted in three images per membrane under a Nikon microscope using a 20 × objective. Both assays were conducted in triplicate.

2.3.5. Tube formation assay of HUVECs

The 96-well plate with Matrigel was solidified at 37 °C for 30 min. HUVECs cultivated with pM, Ti and Mg for 1 week were resuspended and seeded at a density of 2×10^4 cells per well. Matrigel-induced morphological changes in HUVECs cultivated with different extraction media and their tubular networks were photographed after 24 h of incubation. Images were captured and analyzed to measure total tube length. The tube formation assay was conducted in triplicate.

2.3.6. ALP activity of MC3T3-E1 cells

The MC3T3-E1 cells cultivated with pM, Ti and Mg were seeded on 24-well plates (5×10^3 cells per well). The samples were measured at 4, 7, and 14 days of cultivation for quantitative ALP assay. The OD values at 405 nm was tested to determine the ALP activity after incubation with p-nitro-phenyl phosphate (*p*-NPP).

2.3.7. ECM mineralization by MC3T3-E1 cells

Cells cultured with pM, Ti and Mg were evaluated with alizarin red

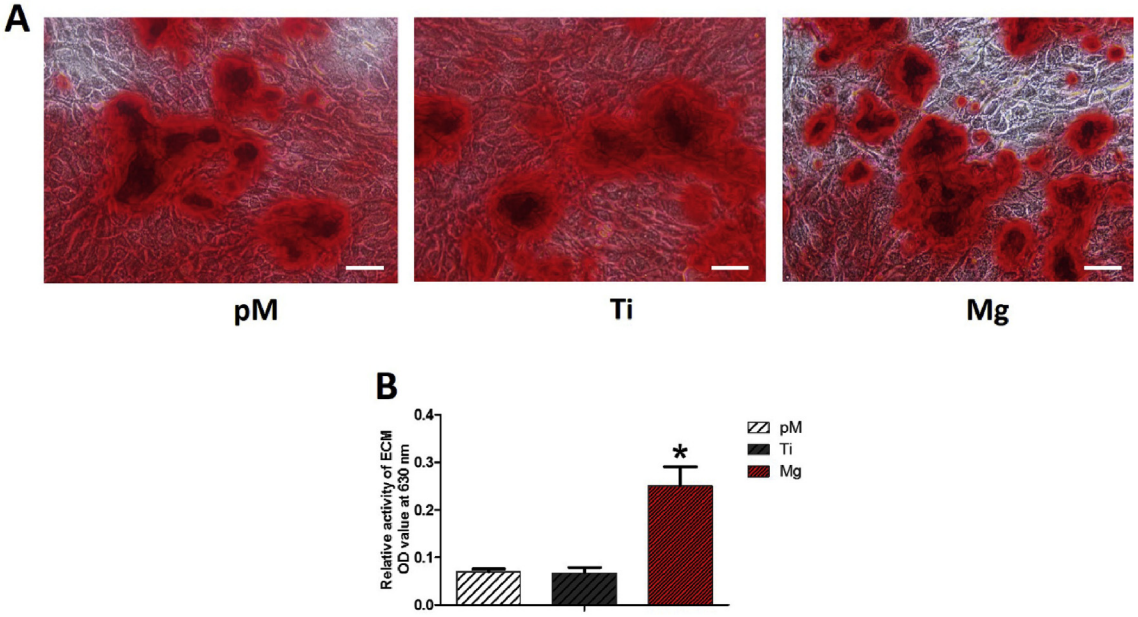

Fig. 8. Analysis of ECM mineralization of MC3T3-E1 cells. Calcium nodes increased in Mg extraction medium-cultured group at 14 days of incubation compared with those of Ti and pM extraction groups. Scale bar = 100 μm. Asterisks (*) indicate statistical significance compared with the Ti and pM groups, $p < 0.05$. Pure complete medium (pM); Ti6Al4V sample extraction (Ti); Mg-coated Ti6Al4V sample extraction (Mg) (n = 3 for each group).

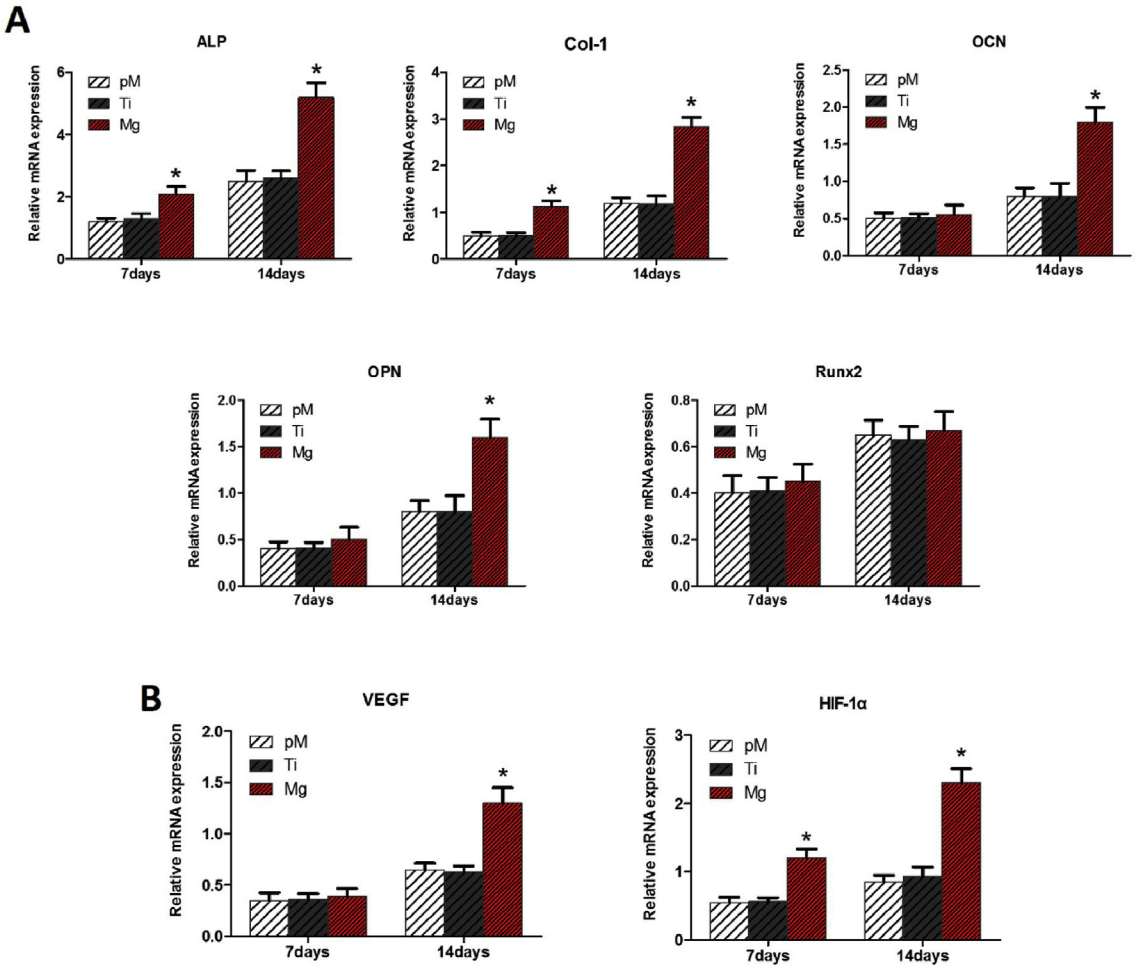

Fig. 9. (A) Relative mRNA expression of osteogenesis-related genes (ALP, Col-1, OCN, OPN, and Runx2) of MC3T3-E1 cells. (B) Relative mRNA expression of angiogenesis-related genes (HIF-1α and VEGF) of HUVECs. Asterisks (*) indicate statistical significance compared with the Ti and pM groups, $p < 0.05$. Pure complete medium (pM); Ti6Al4V sample extraction (Ti); Mg-coated Ti6Al4V sample extraction (Mg) (n = 3 for each group).

staining. Cells were seeded on 24-well plates (4×10^3 cells per well), and cultured using pM, Ti and Mg with osteogenic medium after cell adherence. After 14 days of incubation, cells were stained with alizarin red solution. The absorbance was measured at 630 nm.

2.3.8. Quantitative real-time PCR

In brief, MC3T3-E1 cells (4×10^4 per well) and HUVECs (3×10^4 per well) were seeded on 24-well plates cultured with pM, Ti and Mg. The expression levels of ALP, Col-1, OCN, rRunx2, OPN, HIF-1α, and VEGF were determined after 7 days and 14 days of incubation. Total RNA was extracted and determined and measured. GAPDH was used as control. Table 1 showed the primer sequences.

2.4. In vivo studies

2.4.1. Animals and surgical procedures

To examine early vascularization and long-term bone formation effects *in vivo*, 42 New Zealand white rabbits (3 ± 0.5 kg) were divided into two groups randomly (Ti and Mg). All animal experiments were performed in strict accordance with the Fourth Military Medical University animal ethics committee guidelines. The rabbits were randomly assigned to 7 time points (2, 4, and 8 weeks for vascularization test; 12 weeks for sequential fluorochrome labeling; 6, 9, and 12 months for osteogenesis evaluation and n = 6 rabbits for each time point). The rabbit surgical procedures were performed according to the protocol we previously established [17]. In brief, the rabbits were narcotized and the lateral femoral epicondyles were exposed. Ø5 mm × L10 mm cylindrical defects were made and implanted with bare Ti6Al4V and Mg-coated Ti6Al4V scaffolds randomly (supporting information, Fig. S1). Antibiotics were applied twice a day for 3 days after surgery.

2.4.2. Sequential fluorochrome labeling

In order to monitor the mineralization process around the scaffolds, 25 mg/kg calcein, 30 mg/kg alizarin red S, and 50 mg/kg tetracycline hydrochloride were injected intramuscularly and sequentially at 3, 6, and 9 weeks after implantation [41]. After 12 weeks of surgery, femoral epicondyle samples were fixed for 2 weeks (75% ethanol) before histotomy. Histological sections were prepared, and images were obtained.

2.4.3. Microangiography of rabbit

At each time point, the rabbits used for microangiography were narcotized. The abdominal aorta and postcava were exposed with a median abdominal incision. Both postcava and abdominal aorta were cut and ligated at the proximal end (supporting information, Fig. S2). A tube was inserted into the abdominal aorta, and normal saline with heparin sodium (50 IU/mL) was used to rinse the lower limb blood vessels with an electric syringe. After about a 1-L normal saline rinse, 500 mL 10% formaldehyde was applied to fix the vessels of lower limbs through the abdominal aorta. Subsequently, 50 mL of Microfil® silicone rubber injection compound was injected through the abdominal aorta to perfuse lower limb vessels (2 mL/min). All samples were harvested

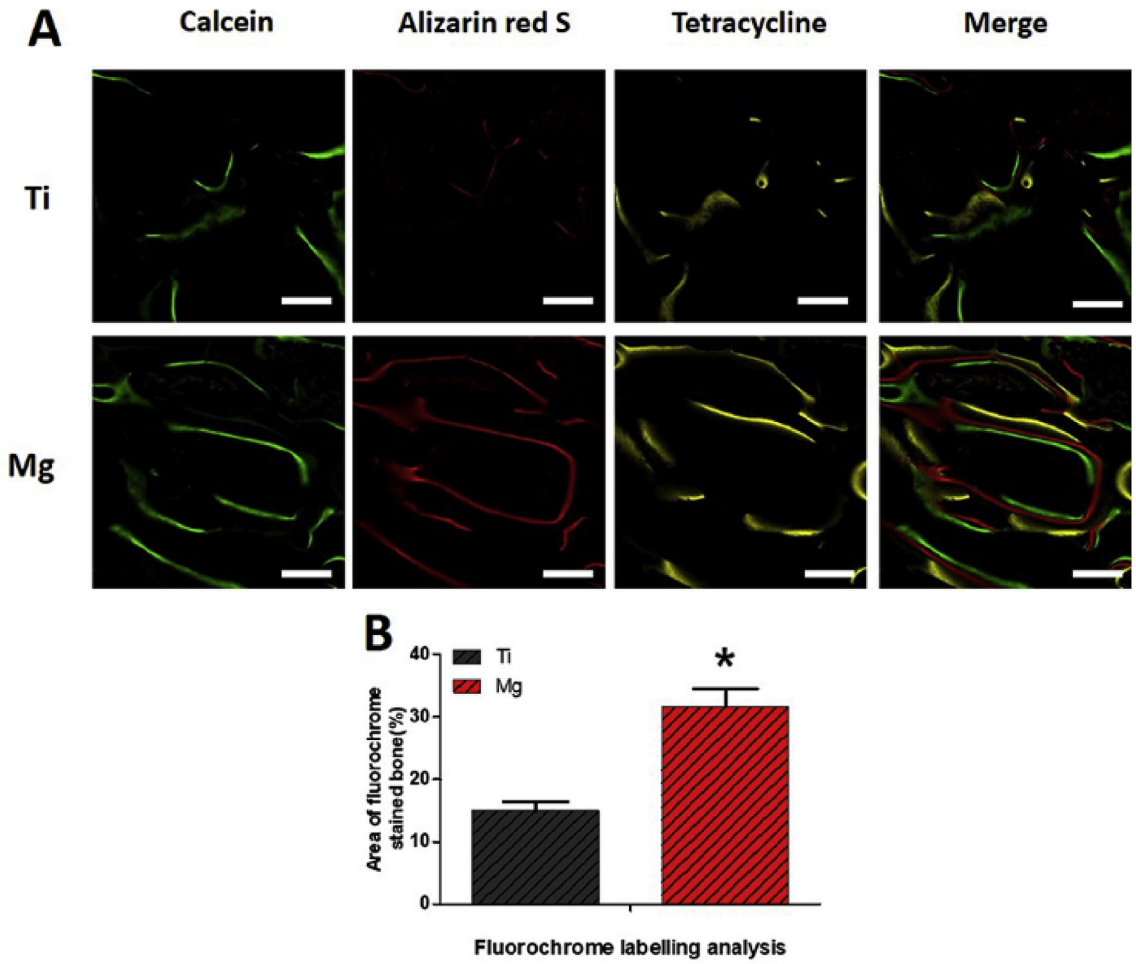

Fig. 10. Sequential fluorescent labeling of Mg-coated Ti6Al4V scaffold (Mg) and bare Ti6Al4V scaffold (Ti) 12 weeks after implantation. Green, red, and yellow represent labeling by calcein, alizarin red S, and tetracycline, respectively. Asterisks (*) indicate statistical significance compared with the bare Ti6Al4V scaffold, $p < 0.05$ (n = 3 for each group, scale bar = 200 μm).

and fixed for 2 weeks (75% ethanol). After that, 10% EDTA was used as a decalcifying solution to treat all samples for 2 months before micro-CT scan.

2.5. Micro-computed tomography evaluation

All samples were scanned to do the micro-computed tomography analysis. For new bone formation analysis, the sample area was set as the region of interest (ROI). A 2 mm range around the micro-angiography sample was set as the ROI for vascularization evaluation. The percentage of newly formed bone volume and blood vessel volume were calculated as bone volume/total scaffolds volume (BV/TV) and blood vessel volume/total volume (BVV/TV), respectively.

2.6. Quantitative histological analysis

The samples were dehydrated and polymerized after micro-computed tomography analysis. After polymerization, serial transverse sections (70-mm-thick) were prepared and stained with Van Gieson's stain according to protocol. All the sections were examined, and images were obtained. Volumes of newly formed bone were calculated and compared statistically.

2.7. Statistical analysis

The quantitative results were presented as the means ± SEM for each group. A one-way ANOVA test was used to perform the statistical analysis among different groups using PASW Statistics 19.0 software. A p value < 0.05 was considered statistically significant. GraphPad Prism 6.0 software was used to plot graphs.

3. Results

3.1. Characterization and degradation of Mg-coating

The surface characterization of the Mg-coated Ti6Al4V scaffold samples before and after immersion into culture medium is shown in Fig. 1. The deposited Mg film had a dense, smooth surface, without flaws. The coating was formed with a uniform size of about 1 μm Mg grains. After immersed in culture medium for 48 h, the Mg coating surface cracked and degraded. The elemental composition of Mg-coated Ti6Al4V samples before and after immersion were determined by energy spectrum analysis. As shown in Fig. 1D, the Mg weight percentage decreased to 11.77% after 48 h of immersion, compared with 28% (Fig. 1B) before immersion.

3.2. In vitro studies on effect of Mg extraction on MC3T3-E1cells and HUVECs

3.2.1. Effect of Mg extraction on cell proliferation and viability

To assess MC3T3-E1 cells and HUVECs cells viability and proliferation co-cultured with pM, Ti, and Mg extraction, an alamarBlue colorimetric assay was applied after cultivation. Both cells proliferated with the increase of cultivation time (Fig. 2A and B). Significantly

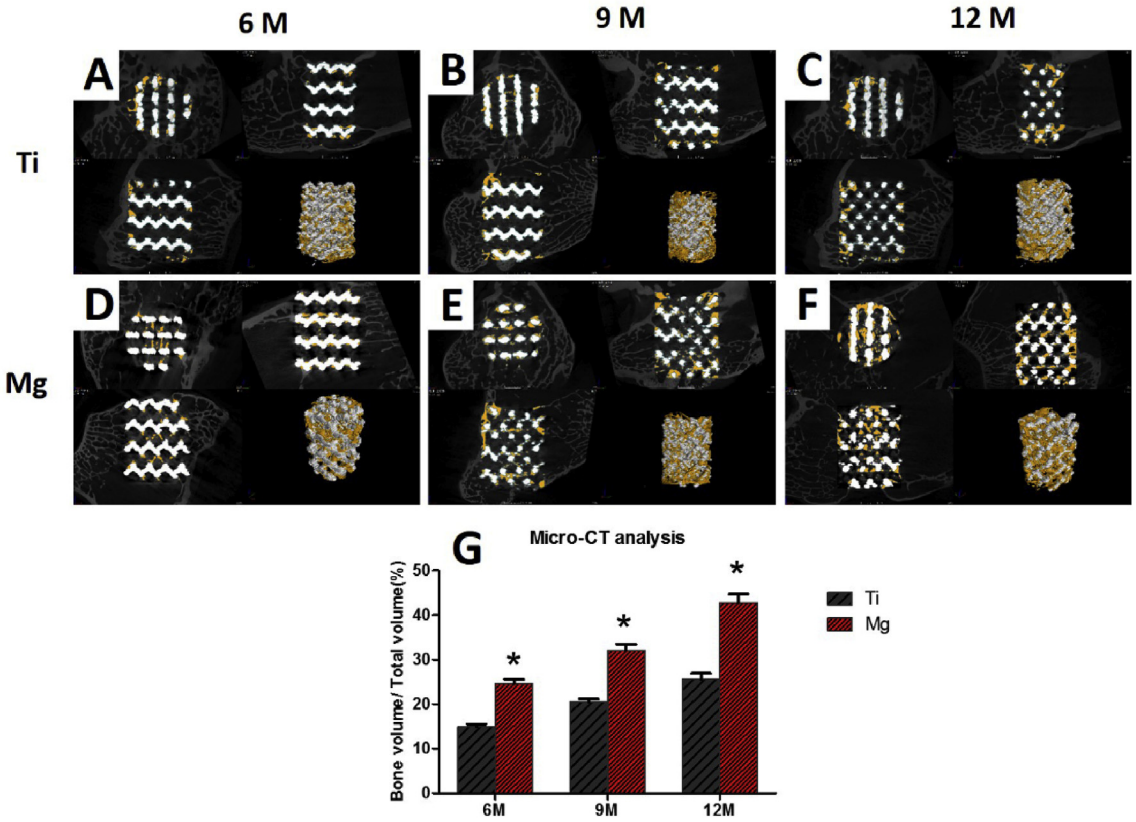

Fig. 11. Micro-CT images of bare Ti6Al4V (A, B, C) and Mg-coated Ti6Al4V (D, E, F) scaffolds after 6, 9, and 12 months of implantation. The yellow components indicate newly formed bone in these scaffolds. (G) Percentages of regenerated bone volume/total volume (BV/TV) in these scaffolds. Asterisks (*) indicate statistical significance compared with the bare Ti6Al4V scaffold, $p < 0.05$ (n = 3 for each group).

higher rate of proliferations of both cells were observed in Mg group than those in Ti and pM groups at 4, 7, and 14 days ($p < 0.05$). On the first day of incubation, no significant proliferation difference was observed among Ti, pM and Mg groups on first day of incubation ($p > 0.05$). No evidence of cell proliferation difference was found between group Ti and pM ($p > 0.05$).

The cell proliferation and viability were also validated by Calcein-AM/PI double staining. Under a confocal microscope, living MC3T3-E1 cells and HUVECs showed bright green fluorescence (Fig. 3). Further quantitative analysis demonstrated that high cell density was maintained in the Mg group (815 ± 53 cells/mm^2 in MC3T3-E1 cells, 910 ± 60 cells/mm^2 in HUVECs) compared with those in the Ti group (580 ± 73 cells/mm^2 in MC3T3-E1 cells, 620 ± 60 cells/mm^2 in HUVECs) and pM group (595 ± 80 cells/mm^2 in MC3T3-E1 cells, 632 ± 43 cells/mm^2 in HUVECs) ($p < 0.05$). Overall, significantly fewer dead cells with small and round morphology were observed based on red fluorescence in the Mg group (Fig. 3C, F). These results revealed that Mg-coated Ti6Al4V was capable of sustaining the high proliferation ability and viability of both cells (Fig. 3G and H).

3.2.2. Effect of Mg extraction on adhesions of MC3T3-E1 cells and HUVECs

The morphologies of these two cells, which reveal cell adhesion behavior, were investigated with staining for F-actin, vinculin, and nuclei. MC3T3-E1 cells (Fig. 4A) and HUVECs (Fig. 4D) cultivated with Mg extraction had better spread than those of the Ti and pM groups. Mg extraction group had a much higher overall cell area to nucleus area (CN ratio) (Fig. 4B, E) ($p < 0.05$). The organization of the cytoskeleton in the Mg group was better compared with those in the Ti and pM groups. Additionally, a higher fluorescence intensity of vinculin staining was found in cells from the Mg group than in those from the Ti and pM groups (Fig. 4C, F). Vinculin was distributed in both the cytoplasm and cell edges in the Mg group, which may result in better cell adhesion.

3.2.3. Effect of Mg extraction on wound-healing and transwell abilities of HUVECs

The motility and migration activities of HUVECs were tested with wound-healing and Transwell assays. Migratory potential increased in the Mg extraction-treated HUVECs compared with those from the Ti and pM groups, as indicated by wound distance (Fig. 5A). Wounds almost fully recovered in the Mg extraction-treated HUVEC group 48 h post scratch, which was much faster than those in the Ti and pM groups ($p < 0.05$). No evidence of wound distance difference at each time point were found between Ti and pM groups ($p > 0.05$).

Similarly, the invasion ability of HUVECs, which was assessed using Transwell invasion chamber assay, was markedly enhanced after treatment with Mg extraction (Fig. 5C). After 48 h of cultivation, the Mg extraction-treated cells invaded through the invasion chamber membrane to a greater extent (212 ± 20) than those treated with Ti (70 ± 18) and pM (65 ± 12) extractions (both $p < 0.05$). Meanwhile, no evidence of difference was found between Ti and pM groups ($p > 0.05$). Collectively, these data suggest that treatment of HUVECs with Mg extraction results in the enhancement of motility and migration abilities.

3.2.4. Effect of Mg extraction on tube formation ability of HUVECs

As one of the characteristic of HUVECs, tube formation indicates the *in vitro* tubulogenesis ability of HUVECs. Compared with these in the Ti extraction and pM groups after 24 h cultivation, a significantly increased number of tubes as well as vessel branch points were detected in the Mg extraction-treated group (Fig. 6, $p < 0.05$). Compared with

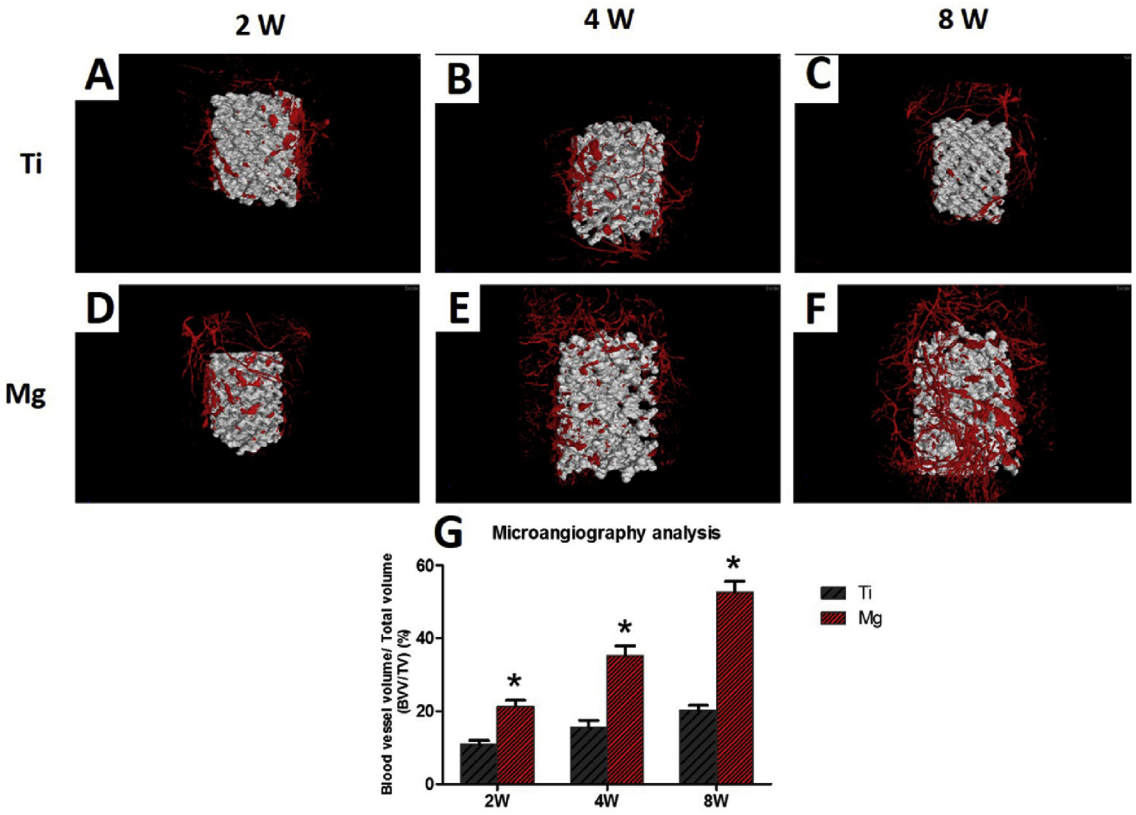

Fig. 12. Microangiography analysis of newly formed blood vessel around the scaffolds. The 2 mm area around the scaffold was chose as ROI, and the blood vessel volume/total volume BVV/TV was calculated. (G)Percentages of regenerated bone volume/total volume BVV/TV in these scaffolds. Asterisks (*) indicate statistical significance compared with the bare Ti6Al4V scaffold, $p < 0.05$ (n = 3 for each group).

Ti extraction and pM treated HUVECs, the Mg extraction-treated HUVECs showed 120% increase in formation of tube-like capillaries (Fig. 6B). The tube length and branch points were assessed as angiogenic parameters in this work. No evidence of tube length and branch points difference were found between Ti and pM groups ($p > 0.05$). Together, these data confirm that Mg extraction treatment possesses the ability to increase the tubulogenesis of HUVECs.

3.2.5. Effect of Mg extraction on ALP activity of MC3T3-E1 cells

A significantly higher ALP activity was observed in Mg extraction treated group throughout the cultivation period than the Ti extraction and pM groups (both $p < 0.05$, Fig. 7, supporting information Fig. S3). With regard to the Mg extraction group (0.48 ± 0.4 μmol/μg total protein), a slightly higher ALP activity was observed than in the Ti (0.41 ± 0.2 μmol/μg total protein) and pM (0.4 ± 0.1 μmol/μg total protein) groups at day 4, but the statistical analysis revealed no difference ($p > 0.05$). Seven days after incubation, the ALP activity of Mg extraction treated MC3T3-E1 cells (2.1 ± 0.4 μmol/μg total protein) markedly increased by about 40% compared with those Ti extraction and pM treated cells (both $p < 0.05$). No evidence of increase difference at 7 and 14 days were found between Ti and pM groups ($p > 0.05$). These quantitative analysis results suggest Mg extraction had long-term stimulating effect on the ALP activity of MC3T3-E1 cells.

3.2.6. Effect of Mg extraction on ECM of MC3T3-E1 cells

ECM mineralization in Mg extraction group increased compared with those in both the Ti extraction and pM groups (Fig. 8). According to the ECM staining images, at 14 days of incubation, less calcium nodes appeared on the Ti extraction and pM groups, and the number of calcium nodes increased on Mg extraction group. These collective data reveal that Mg extraction promotes MC3T3-E1 cells ECM mineralization.

3.2.7. Osteogenesis-related and angiogenesis-related gene expression

In the Mg extraction group, high levels of osteogenesis-related genes ALP and Col-1 expression of MC3T3-E1 cells were found at 7 and 14 days of incubation compared with those in both Ti extraction and pM groups ($p < 0.05$, Fig. 9A). Significantly higher OCN and OPN gene expression levels in the Mg extraction group were observed at 14 days. Interestingly, there were no significant changes in Runx2 expression among the three groups at 7 and 14 days ($p > 0.05$). No significant difference were found between the Ti extraction and pM groups at 7 and 14 days.

The levels of angiogenesis-related genes HIF-1α and VEGF in HUVECs increased significantly in the Mg extraction group at 14 days of incubation ($p < 0.05$, Fig. 9B). At 7 days of incubation, no evidence of VEGF gene expression difference among these three groups, while HIF-1α expression in the Mg extraction group was much higher than those in the Ti extraction and pM groups ($p < 0.05$). At 7 and 14 days, HIF-1α and VEGF expression between the Ti extraction and pM groups did not show any significant difference ($p > 0.05$).

3.3. In vivo studies of Mg-coated Ti6Al4V scaffold

3.3.1. Sequential fluorochrome labeling analysis

Calcein was observed on a wider area surrounding the Mg-coated Ti6Al4V scaffolds compared with that in the bare Ti6Al4V scaffold. Alizarin red was deposited onto a wide area along with calcein in both scaffolds. A more intense and wider distribution of red fluorescence was observed in the Mg-coated Ti6Al4V scaffolds. As for tetracycline, a large and long yellow line extended along the alizarin red area, indicating more bone formation. Newly formed bone grew from the existing bone surface region toward the scaffold (Fig. 10A). Statistical results revealed that new bone formation in the Mg-coated Ti6Al4V scaffold (31.5 ± 5.2%) was significantly higher than in the bare Ti6Al4V

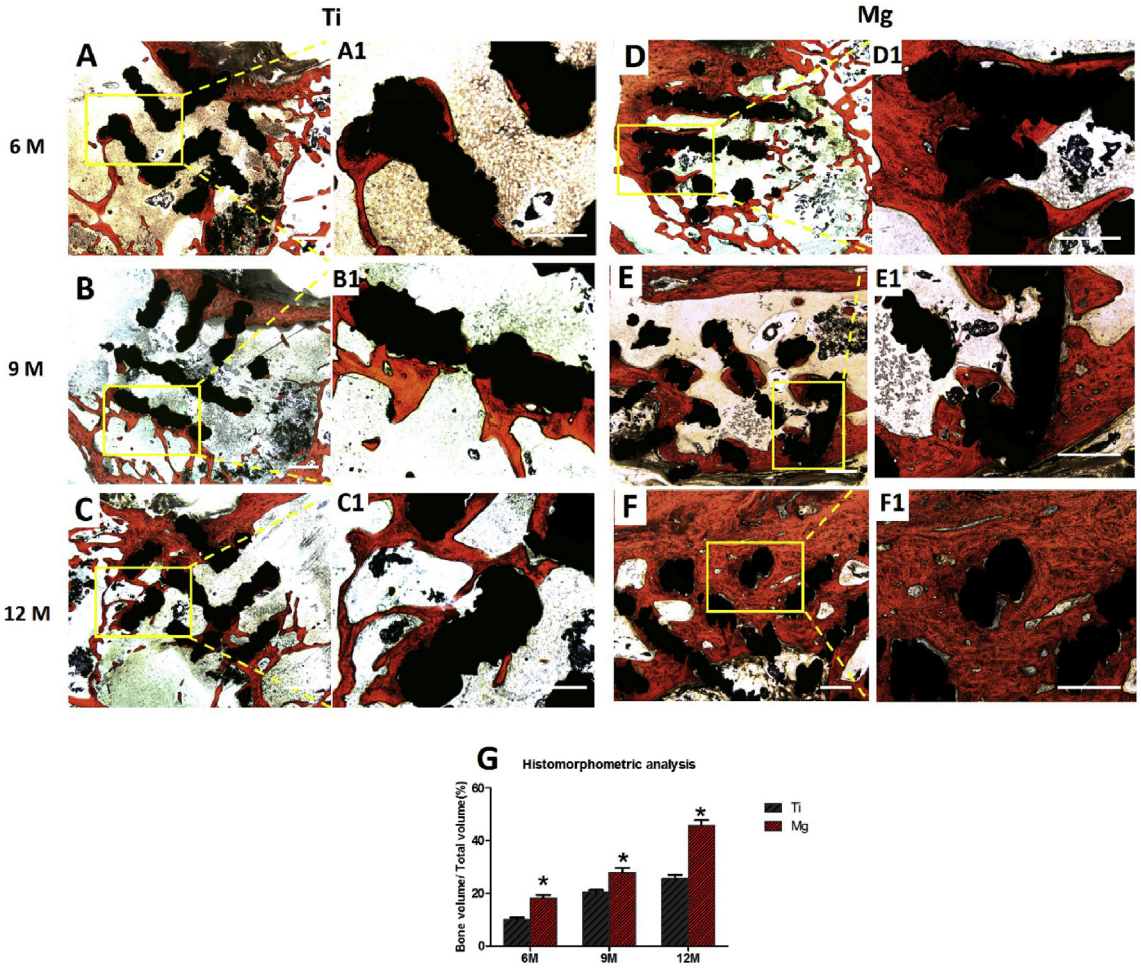

Fig. 13. Van-Gieson staining histological sections (A–F) and (G) quantitative analysis of the bare Ti6Al4V and Mg-coated Ti6Al4V scaffolds at 6, 9 and 12 months postoperation. The red-stained tissue indicates newly formed bone. Asterisks (*) indicate statistical significance compared with the bare Ti6Al4V scaffold, $p < 0.05$ (n = 3 for each group, scale bar = 200 μm).

scaffold (15 ± 2.4%) at 12 weeks post operation ($p < 0.05$, Fig. 10B).

3.3.2. Micro-CT evaluation of newly formed bone and vessels

The new bone tissues (yellow) were found to spread from the margin of scaffolds (white) into the center. The percentage of BV/TV in both scaffold increased with implantation time (Fig. 11). In the bare Ti6Al4V scaffold, new bone was observed mainly around the periphery of the scaffold, while the Mg-coated Ti6Al4V scaffold had more favorable new bone ingrowth into the scaffold. At 6 months post-operation, a significantly higher BV/TV value was found in the Mg-coated Ti6Al4V scaffold (24.5 ± 1.8%) compared with that in the bare Ti6Al4V scaffold (14.9 ± 0.95%, $p < 0.05$). After 9 and 12 months of implantation, the Mg-coated Ti6Al4V scaffold exhibited much higher ability of promoting new bone formation and ingrowth than the bare Ti6Al4V scaffold did ($p < 0.05$). These collective results showed that the Mg-coated Ti6Al4V scaffold greatly promotes bone regeneration.

After microangiography and decalcification, newly formed blood vessels were also characterized by micro-CT. The 2-mm area around the scaffold was chose as an ROI, and the blood vessel volume/total volume (BVV/TV) was calculated. Based on the collected images, blood vessels had an increased number and volume growth around the Mg-coated Ti6Al4V scaffold compared with those around the bare Ti6Al4V scaffold. The blood vessel volume increased with implantation time. A significantly higher BVV/TV value was found in the Mg-coated Ti6Al4V scaffold group (21.2 ± 3.2%) compared with that in the bare Ti6Al4V scaffold group (10.9 ± 1.8%, $p < 0.05$) 2 weeks after implantation (Fig. 12). At 4 weeks, the BVV/TV value was 35.3 ± 4.5% in the Mg-coated Ti6Al4V scaffold group, which was higher than that in the bare Ti6Al4V scaffold group (15.5 ± 3.4%, $p < 0.05$). The same result was observed 8 weeks after implantation, revealing that the Mg-coated Ti6Al4V scaffold could accelerate blood vessel formation around the scaffold, which may lead to better vascularization inside the scaffold.

3.3.3. Histological analysis

The newly formed bone (red) ingrowth appeared to directly emanate from the bone defect border toward the scaffolds. There were no inflammatory reaction and gas cavities found in any group. The volume of regenerated bone and thickness of trabeculae increased with implantation time in both groups. Well integration was observed between the new bone and the Mg-coated Ti6Al4V scaffolds at each time points (Fig. 13). A large volume of newly formed bone deep inside the Mg-coated Ti6Al4V scaffold was observed, while new bone in the bare Ti6Al4V scaffold was limited and isolated. The histomorphometric analysis revealed a much higher bone volumes in Mg-coated Ti6Al4V group at 6, 9, and 12 months compared with bare Ti6Al4V group. These data collectively demonstrate that Mg-coated Ti6Al4V scaffold exhibits the ability of better osteogenesis and osteointegration.

4. Discussion

Porous titanium scaffolds with controllable geometry, suitable porosity, and favorable pore size are the materials of choice for use as

substitutes for bone repair [42–45]. Recently, manufacturing porous titanium scaffolds with distinguished mechanical properties, less stress shielding, and better new bone ingrowth have received considerable attention [46,47]. Supply of nutrients and oxygen from blood vessels is of vital importance in osteogenesis and survival of porous titanium scaffolds [48,49]. New blood vessel formation or angiogenesis is required for the scaffold to be functional. Although there has been considerable development of surface modifications of porous titanium scaffolds, insufficient bone growth and blood vessel ingrowth into the porous titanium scaffold have limited their further application. Therefore, a biofunctional coating with both osteogenesis and angiogenesis properties is required for porous titanium scaffold long term fixation and survival which are crucial for their clinical applications.

Recent studies have reported the prominent advantages of Mg and its alloys, including biodegradability and biocompatibility, and they have been considered to be revolutionized implant materials [50–52]. Some previous studies reported the *in vitro* Mg alloy degradation and corrosion could increase the pH of the culture medium, which may affect cell survival [53–55]. In theory, the human body cannot unlimitedly intake any metal. Toxic reactions from Mg alloy degradation happen only beyond the tolerance limit [56,57]. In this study, Mg was applied as a coating on porous Ti6Al4V scaffold with relatively small amount of Mg usage compare to Mg-based alloy. The biocompatibility and toxicity of the scaffold are determined by the release amount of Mg ion, which is related to the Mg volume and corrosion rate of the coating. The pH change and hydrogen release caused by degradation of such amount of Mg were proved to have no harm on surround tissue in this study.

After immersion in culture medium for 48 h, the Mg coating surface became coarse, cracked and degraded. The Mg weight percentage decreased from 28% to 11.77% after 48 h of immersion. *In vitro* studies revealed that the Mg-coated Ti6Al4V extraction had favorable biocompatibility. High cell proliferation and viability were found when incubated with Mg extraction compared with these of bare Ti6Al4V extraction and pure medium. Vinculin is a vital component for cell focal adhesion, which plays a crucial role in cell attachment, migration, and formation of cytoskeleton actin [6,58]. Furthermore, MC3T3-E1 cells and HUVECs cultured with Mg extraction showed an increased intensity of vinculin staining as well as more lamellipodia extensions than those cultured with bare Ti6Al4V extraction and pure medium.

Cell differentiation is also critical for new bone formation except for cell proliferation and adhesion. ALP activity was analyzed and was significantly higher throughout the observation period in the Mg extraction group. Meanwhile, a large number of calcium nodes of ECM mineralization were observed in Mg extraction group. At 7 and 14 days of incubation, ALP and COL-1 gene were highly expressed in the Mg extraction-cultured MC3T3-E1 cells compared with those in both Ti extraction and pM-cultured MC3T3-E1 cells. However, OCN and OPN gene expressions only increased at 14 days in Mg extraction cultivation. Interestingly, there was no change in Runx2 gene expression among all groups at each observation point. These results collectively indicate that Mg extraction possess the ability of promoting osteogenic differentiation of MC3T3-E1 cells, which is consistent with the previous studies on Mg alloy and Mg substrate [33,59,60].

In addition to osteogenesis, early vascularization or angiogenesis is of great importance for scaffold survival and will eventually facilitate osteogenesis. HUVECs migration is essential for angiogenesis. In this study, a significant increase of migratory potential was observed on Mg extraction-treated HUVECs, as demonstrated by the wound-healing assay. Wounds almost fully recovered in the Mg extraction-treated HUVECs group 48 h post scratch. Similarly, the invasive ability of HUVECs was markedly enhanced after treatment with Mg extraction, as assessed by Transwell invasion chamber assays. After 48 h of cultivation, a higher rate of cell invaded through the invasion chamber membrane was observed in the Mg extraction-treated group. Tube formation is one of the characteristics of HUVECs that indicates the *in vitro* tubulogenesis ability. Compared with those in the Ti extraction and pM groups after 24 h of cultivation, a significantly increased number of tubes and vessel branch points were observed in the Mg extraction group. However, the Ti and pM extraction groups had no statistical difference in HUVECs motility, migration activity, and tubulogenesis. Collectively, these data suggest that HUVECs treated with Mg extraction can result in the enhancement of motility, migration, and tubulogenesis ability. Compared with Ti extraction and pM groups, higher expression of HIF-1α and VEGF gene were found in the Mg extraction group at 14 days of incubation. HIF-1α is a transcription factor that promotes angiogenesis by simulating hypoxic conditions and promoting the transcription of VEGF, which is an important proangiogenic factor and angiogenesis-signaling gene [21,61]. The increased expression of HIF-1α results in enhanced VEGF, which is in agreement with the common opinion that Mg plays a crucial role in angiogenesis by activating HIF-1α transcriptional activity [62,63]. Mg was reported to increase the activity of magnesium transporter subtype 1 (MagT1), which is a cellular component essential to vertebrate Mg influx [21,64]. Thus, Mg extraction from Mg-coated Ti6Al4V scaffold may up-regulate the expression of MagT1, which results in Mg influx, and then stimulates the VEGF transcription of HUVECs via activation of HIF-1α.

Along with the *in vitro* tests of the Mg-coated Ti6Al4V scaffold, the *in vivo* early vascularization and long-term bone formation effects of the Mg-coated Ti6Al4V scaffold were evaluated using a rabbit femoral condylar defect model. Sequential fluorochrome markers were administered in rabbits for 12 weeks to monitor new bone formation of the scaffold. Quantitative analysis revealed that newly formed bone after 12 weeks of operation in Mg-coated Ti6Al4V scaffold group was significantly higher than bare Ti6Al4V scaffold group. The same outcome was observed with the micro-CT scan. Compared with bare Ti6Al4V scaffold at 6 months post-operation, the BV/TV value of Mg-coated Ti6Al4V scaffold was significantly higher. The newly formed bone in both groups increased with implantation time. Compared with bare Ti6Al4V scaffold, the newly formed bone volumes were much higher in Mg-coated Ti6Al4V group at 6, 9, and 12 months post-operation. These data collectively demonstrate that better osseointegration and osteogenesis are achieved with the Mg-coated Ti6Al4V scaffold.

In this study, microangiography analysis of vascularization around scaffolds was applied for the first time. After microangiography and decalcification, newly formed blood vessels were also characterized by micro-CT. As the Microfil® silicone rubber injection compounds and Ti6Al4V have nearly identical CT value, it is very difficult to distinguish the blood vessels from Ti6Al4V. Therefore, the 2-mm area around the scaffold was chosen as an ROI to indirectly reflect the vascularization. Based on the collected images, blood vessels proliferated with implantation time and increased in number and volume growth around the Mg-coated Ti6Al4V scaffold compared with those in the bare Ti6Al4V scaffold. The BVV/TV value was significantly higher in the Mg-coated Ti6Al4V scaffold group (21.2 ± 3.2%) compared with that in the bare Ti6Al4V scaffold group (10.9 ± 1.8%) at 2 weeks. At 4 weeks, the BVV/TV value was 35.3 ± 4.5% in the Mg-coated Ti6Al4V scaffold group and 15.5 ± 3.4% in the bare Ti6Al4V scaffold group. The same result was observed at 8 weeks, revealing that the Mg-coated Ti6Al4V scaffold can accelerate early blood vessel formation around the scaffold, which indirectly reflects better vascularization inside the scaffold.

Thus, we demonstrate that Mg coating is a promising surface modification on porous Ti6Al4V scaffolds for orthopedic applications in this work. Mg coating on Ti6Al4V scaffold has enlarged the scope of applying Mg for weight bearing in orthopedic application. The Mg-coated Ti6Al4V scaffold exhibits favorable osteogenic and angiogenic properties *in vitro* and increases long-term bone formation and early vascularization *in vivo*. However, future studies of specific molecular mechanisms underlying osteogenesis and angiogenesis with Mg-coated Ti6Al4V are necessary.

5. Conclusion

In this study, a biofunctional Mg-coated Ti6Al4V shows favorable osteogenic and angiogenic properties *in vitro*. Cell proliferation, viability, and adhesion are enhanced by Mg extraction compared with bare Ti6Al4V extraction. ALP activity, ECM mineralization, and osteogenesis-related gene expression of MC3T3-E1 cells indicate better osteogenesis in the Mg extraction group. Wound-healing, Transwell, and tube formation assays as well as angiogenesis-related gene expression show that Mg extraction can increase the angiogenesis function of HUVECs. *In vivo* tests using sequential fluorochrome labeling analysis, micro-CT evaluation, and histological examination reveal that the Mg-coated Ti6Al4V scaffold can accelerate early blood vessel formation as well as osseointegration and osteogenesis around and inside the scaffold. Therefore, this novel Mg-coated Ti6Al4V scaffold enlarges the application scope of magnesium and is much promising as bone substitutes for orthopedic applications. Nevertheless, the specific molecular mechanisms underlying osteogenesis and angiogenesis with Mg-coated Ti6Al4V are still not fully elucidated which need to be illuminated in future studies.

CRediT authorship contribution statement

Peng Gao: Conceptualization, Methodology, Validation, Formal analysis, Investigation, Writing - original draft. **Bo Fan:** Methodology, Validation, Formal analysis. **Xiaoming Yu:** Resources, Data curation, Validation. **Wenwen Liu:** Formal analysis, Investigation, Visualization. **Jie Wu:** Methodology, Validation. **Lei Shi:** Investigation, Formal analysis. **Di Yang:** Methodology, Formal analysis. **Lili Tan:** Writing - review & editing. **Peng Wan:** Methodology, Validation. **Yulin Hao:** Formal analysis, Investigation. **Shujun Li:** Resources, Methodology. **Wentao Hou:** Resources, Visualization. **Ke Yang:** Resources, Data curation. **Xiaokang Li:** Writing - review & editing, Funding acquisition. **Zheng Guo:** Supervision, Project administration, Funding acquisition.

Declaration of competing interest

The authors declared no conflict of interest.

This work was financially supported by The National Key Research and Development Program of China (grant number 2017YFC1104901), The National Natural Science Foundation of China (grant number 51871239, 51771227), National Natural Science Foundation of Youth Fund (grant number 51501223).

Appendix A. Supplementary data

Supplementary data to this article can be found online at https://doi.org/10.1016/j.bioactmat.2020.04.019.

References

[1] S.R. Shin, P. Tornetta 3rd, Donor site morbidity after anterior iliac bone graft harvesting, J. Orthop. Trauma 30 (6) (2016) 340–343, https://doi.org/10.1097/BOT.0000000000000551.

[2] G.M. Calori, M. Colombo, E.L. Mazza, S. Mazzola, E. Malagoli, G.V. Mineo, Incidence of donor site morbidity following harvesting from iliac crest or RIA graft, Injury 45 (Suppl 6) (2014) S116–S120, https://doi.org/10.1016/j.injury.2014.10.034.

[3] C.M. Murphy, M.G. Haugh, F.J. O'Brien, The effect of mean pore size on cell attachment, proliferation and migration in collagen-glycosaminoglycan scaffolds for bone tissue engineering, Biomaterials 31 (3) (2010) 461–466, https://doi.org/10.1016/j.biomaterials.2009.09.063.

[4] X. Li, X.Y. Ma, Y.F. Feng, Z.S. Ma, J. Wang, T.C. Ma, W. Qi, W. Lei, L. Wang, Osseointegration of chitosan coated porous titanium alloy implant by reactive oxygen species-mediated activation of the PI3K/AKT pathway under diabetic conditions, Biomaterials 36 (2015) 44–54, https://doi.org/10.1016/j.biomaterials.2014.09.012.

[5] M. Diefenbeck, C. Schrader, F. Gras, T. Muckley, J. Schmidt, S. Zankovych, J. Bossert, K.D. Jandt, A. Volpel, B.W. Sigusch, H. Schubert, S. Bischoff, W. Pfister, B. Edel, M. Faucon, U. Finger, Gentamicin coating of plasma chemical oxidized titanium alloy prevents implant-related osteomyelitis in rats, Biomaterials 101 (2016) 156–164, https://doi.org/10.1016/j.biomaterials.2016.05.039.

[6] Y. Li, W. Yang, X. Li, X. Zhang, C. Wang, X. Meng, Y. Pei, X. Fan, P. Lan, C. Wang, X. Li, Z. Guo, Improving osteointegration and osteogenesis of three-dimensional porous Ti6Al4V scaffolds by polydopamine-assisted biomimetic hydroxyapatite coating, ACS Appl. Mater. Interfaces 7 (10) (2015) 5715–5724, https://doi.org/10.1021/acsami.5b00331.

[7] Y. Cai, X. Wang, C.K. Poh, H.C. Tan, M.T. Soe, S. Zhang, W. Wang, Accelerated bone growth in vitro by the conjugation of BMP2 peptide with hydroxyapatite on titanium alloy, Colloids Surf. B Biointerfaces 116 (2014) 681–686, https://doi.org/10.1016/j.colsurfb.2013.11.004.

[8] R.I.M. Asri, W.S.W. Harun, M. Samykano, N.A.C. Lah, S.A.C. Ghani, F. Tarlochan, M.R. Raza, Corrosion and surface modification on biocompatible metals: a review, Materials science & engineering. C, Materials for biological applications 77 (2017) 1261–1274, https://doi.org/10.1016/j.msec.2017.04.102.

[9] L.T. de Jonge, S.C. Leeuwenburgh, J.G. Wolke, J.A. Jansen, Organic-inorganic surface modifications for titanium implant surfaces, Pharmaceut. Res. 25 (10) (2008) 2357–2369, https://doi.org/10.1007/s11095-008-9617-0.

[10] A. Jemat, M.J. Ghazali, M. Razali, Y. Otsuka, Surface modifications and their effects on titanium dental implants, BioMed Res. Int. 2015 (2015) 791725, https://doi.org/10.1155/2015/791725.

[11] I. Watanabe, S. Kiyosue, C. Ohkubo, T. Aoki, T. Okabe, Machinability of cast commercial titanium alloys, J. Biomed. Mater. Res. 63 (6) (2002) 760–764, https://doi.org/10.1002/jbm.10413.

[12] S. Szmukler-Moncler, D. Perrin, V. Ahossi, G. Magnin, J.P. Bernard, Biological properties of acid etched titanium implants: effect of sandblasting on bone anchorage, J. Biomed. Mater. Res. B Appl. Biomater. 68 (2) (2004) 149–159, https://doi.org/10.1002/jbm.b.20003.

[13] Q. Bi, X. Song, Y. Chen, Y. Zheng, P. Yin, T. Lei, Zn-HA/Bi-HA biphasic coatings on Titanium: fabrication, characterization, antibacterial and biological activity, Colloids Surf. B Biointerfaces 189 (2020) 110813, https://doi.org/10.1016/j.colsurfb.2020.110813.

[14] S. Nishiguchi, S. Fujibayashi, H.M. Kim, T. Kokubo, T. Nakamura, Biology of alkali- and heat-treated titanium implants, J. Biomed. Mater. Res. 67 (1) (2003) 26–35, https://doi.org/10.1002/jbm.a.10540.

[15] T. Wang, L. Wang, Q. Lu, Z. Fan, Changes in the esthetic, physical, and biological properties of a titanium alloy abutment treated by anodic oxidation, J. Prosthet. Dent 121 (1) (2019) 156–165, https://doi.org/10.1016/j.prosdent.2018.03.024.

[16] A. Sobolev, A. Kossenko, K. Borodianskiy, Study of the effect of current pulse frequency on Ti-6Al-4V alloy coating formation by micro arc oxidation, Materials 12 (23) (2019), https://doi.org/10.3390/ma12233983.

[17] X. Li, P. Gao, P. Wan, Y. Pei, L. Shi, B. Fan, C. Shen, X. Xiao, K. Yang, Z. Guo, Novel bio-functional magnesium coating on porous Ti6Al4V orthopaedic implants: in vitro and in vivo study, Sci. Rep. 7 (2017) 40755, https://doi.org/10.1038/srep40755.

[18] X. Zhang, J. Chen, X. Pei, J. Wang, Q. Wan, S. Jiang, C. Huang, X. Pei, Enhanced osseointegration of porous titanium modified with zeolitic imidazolate framework-8, ACS Appl. Mater. Interfaces 9 (30) (2017) 25171–25183, https://doi.org/10.1021/acsami.7b07800.

[19] G. Li, H. Cao, W. Zhang, X. Ding, G. Yang, Y. Qiao, X. Liu, X. Jiang, Enhanced osseointegration of hierarchical micro/nanotopographic titanium fabricated by microarc oxidation and electrochemical treatment, ACS Appl. Mater. Interfaces 8 (6) (2016) 3840–3852, https://doi.org/10.1021/acsami.5b10633.

[20] C. Wang, K. Lin, J. Chang, J. Sun, Osteogenesis and angiogenesis induced by porous beta-CaSiO(3)/PDLGA composite scaffold via activation of AMPK/ERK1/2 and PI3K/Akt pathways, Biomaterials 34 (1) (2013) 64–77, https://doi.org/10.1016/j.biomaterials.2012.09.021.

[21] Y. Yu, G. Jin, Y. Xue, D. Wang, X. Liu, J. Sun, Multifunctions of dual Zn/Mg ion co-implanted titanium on osteogenesis, angiogenesis and bacteria inhibition for dental implants, Acta Biomater. 49 (2017) 590–603, https://doi.org/10.1016/j.actbio.2016.11.067.

[22] M. Lalk, J. Reifenrath, N. Angrisani, A. Bondarenko, J.M. Seitz, P.P. Mueller, A. Meyer-Lindenberg, Fluoride and calcium-phosphate coated sponges of the magnesium alloy AX30 as bone grafts: a comparative study in rabbits, J. Mater. Sci. Mater. Med. 24 (2) (2013) 417–436, https://doi.org/10.1007/s10856-012-4812-2.

[23] R.H. Adams, K. Alitalo, Molecular regulation of angiogenesis and lymphangiogenesis, Nat. Rev. Mol. Cell Biol. 8 (6) (2007) 464–478, https://doi.org/10.1038/nrm2183.

[24] F.Y. Li, B. Chaigne-Delalande, C. Kanellopoulou, J.C. Davis, H.F. Matthews, D.C. Douek, J.I. Cohen, G. Uzel, H.C. Su, M.J. Lenardo, Second messenger role for Mg2+ revealed by human T-cell immunodeficiency, Nature 475 (7357) (2011) 471–476, https://doi.org/10.1038/nature10246.

[25] H.M. Wong, Y. Zhao, F.K.L. Leung, T. Xi, Z. Zhang, Y. Zheng, S. Wu, K.D.K. Luk, K.M.C. Cheung, P.K. Chu, K.W.K. Yeung, Functionalized polymeric membrane with enhanced mechanical and biological properties to control the degradation of magnesium alloy, Adv Healthc Mater 6 (8) (2017), https://doi.org/10.1002/adhm.201601269.

[26] B. Zberg, P.J. Uggowitzer, J.F. Loffler, MgZnCa glasses without clinically observable hydrogen evolution for biodegradable implants, Nat. Mater. 8 (11) (2009) 887–891, https://doi.org/10.1038/nmat2542.

[27] H.F. Li, X.H. Xie, K. Zhao, Y.B. Wang, Y.F. Zheng, W.H. Wang, L. Qin, In vitro and in vivo studies on biodegradable CaMgZnSrYb high-entropy bulk metallic glass, Acta Biomater. 9 (10) (2013) 8561–8573, https://doi.org/10.1016/j.actbio.2013.01.

029.
[28] G. Ciapetti, G. Di Pompo, S. Avnet, D. Martini, A. Diez-Escudero, E.B. Montufar, M.P. Ginebra, N. Baldini, Osteoclast differentiation from human blood precursors on biomimetic calcium-phosphate substrates, Acta Biomater. 50 (2017) 102–113, https://doi.org/10.1016/j.actbio.2016.12.013.
[29] A.K. Teotia, A. Gupta, D.B. Raina, L. Lidgren, A. Kumar, Gelatin-Modified bone substitute with bioactive molecules enhance cellular interactions and bone regeneration, ACS Appl. Mater. Interfaces 8 (17) (2016) 10775–10787, https://doi.org/10.1021/acsami.6b02145.
[30] N.L. D'Elia, C. Mathieu, C.D. Hoemann, J.A. Laiuppa, G.E. Santillan, P.V. Messina, Bone-repair properties of biodegradable hydroxyapatite nano-rod superstructures, Nanoscale 7 (44) (2015) 18751–18762, https://doi.org/10.1039/c5nr04850h.
[31] D. Persaud-Sharma, A. McGoron, Biodegradable magnesium alloys: a review of material development and applications, J. Biomim. Biomater. Tissue Eng. 12 (2012) 25–39 https://doi.org/10.4028/www.scientific.net/JBBTE.12.25.
[32] J. Zhang, X. Ma, D. Lin, H. Shi, Y. Yuan, W. Tang, H. Zhou, H. Guo, J. Qian, C. Liu, Magnesium modification of a calcium phosphate cement alters bone marrow stromal cell behavior via an integrin-mediated mechanism, Biomaterials 53 (2015) 251–264, https://doi.org/10.1016/j.biomaterials.2015.02.097.
[33] Y. Okuzu, S. Fujibayashi, S. Yamaguchi, K. Yamamoto, T. Shimizu, T. Sono, K. Goto, B. Otsuki, T. Matsushita, T. Kokubo, S. Matsuda, Strontium and magnesium ions released from bioactive titanium metal promote early bone bonding in a rabbit implant model, Acta Biomater. 63 (2017) 383–392, https://doi.org/10.1016/j.actbio.2017.09.019.
[34] J.A. Kim, H.S. Yun, Y.A. Choi, J.E. Kim, S.Y. Choi, T.G. Kwon, Y.K. Kim, T.Y. Kwon, M.A. Bae, N.J. Kim, Y.C. Bae, H.I. Shin, E.K. Park, Magnesium phosphate ceramics incorporating a novel indene compound promote osteoblast differentiation in vitro and bone regeneration in vivo, Biomaterials 157 (2017) 51–61, https://doi.org/10.1016/j.biomaterials.2017.11.032.
[35] L. Cao, W. Weng, X. Chen, J. Zhang, Q. Zhou, J. Cui, Y. Zhao, J.W. Shin, J. Su, Promotion of in vivo degradability, vascularization and osteogenesis of calcium sulfate-based bone cements containing nanoporous lithium doping magnesium silicate, Int. J. Nanomed. 12 (2017) 1341–1352, https://doi.org/10.2147/IJN.S124965.
[36] H. Bao, F. Lv, T. Liu, A pro-angiogenic degradable Mg-poly(lactic-co-glycolic acid) implant combined with rhbFGF in a rat limb ischemia model, Acta Biomater. 64 (2017) 279–289, https://doi.org/10.1016/j.actbio.2017.09.033.
[37] M. Badar, H. Lunsdorf, F. Evertz, M.I. Rahim, B. Glasmacher, H. Hauser, P.P. Mueller, The formation of an organic coat and the release of corrosion microparticles from metallic magnesium implants, Acta Biomater. 9 (7) (2013) 7580–7589, https://doi.org/10.1016/j.actbio.2013.03.012.
[38] F. Seuss, S. Seuss, M.C. Turhan, B. Fabry, S. Virtanen, Corrosion of Mg alloy AZ91D in the presence of living cells, J. Biomed. Mater. Res. B Appl. Biomater. 99 (2) (2011) 276–281, https://doi.org/10.1002/jbm.b.31896.
[39] J. Parthasarathy, B. Starly, S. Raman, A. Christensen, Mechanical evaluation of porous titanium (Ti6Al4V) structures with electron beam melting (EBM), Journal of the mechanical behavior of biomedical materials 3 (3) (2010) 249–259, https://doi.org/10.1016/j.jmbbm.2009.10.006.
[40] D.T. Chou, D. Hong, P. Saha, J. Ferrero, B. Lee, Z. Tan, Z. Dong, P.N. Kumta, In vitro and in vivo corrosion, cytocompatibility and mechanical properties of biodegradable Mg-Y-Ca-Zr alloys as implant materials, Acta Biomater. 9 (10) (2013) 8518–8533, https://doi.org/10.1016/j.actbio.2013.06.025.
[41] T. Lu, J. Wen, S. Qian, H. Cao, C. Ning, X. Pan, X. Jiang, X. Liu, P.K. Chu, Enhanced osteointegration on tantalum-implanted polyetheretherketone surface with bone-like elastic modulus, Biomaterials 51 (2015) 173–183, https://doi.org/10.1016/j.biomaterials.2015.02.018.
[42] S. Tunchel, A. Blay, R. Kolerman, E. Mijiritsky, J.A. Shibli, 3D printing/additive manufacturing single titanium dental implants: a prospective multicenter study with 3 Years of follow-up, Int J Dent 2016 (2016) 8590971, https://doi.org/10.1155/2016/8590971.
[43] S.W. Carlson, D.D. Goetz, S.S. Liu, J.J. Greiner, J.J. Callaghan, Minimum 10-year follow-up of cementless total hip arthroplasty using a contemporary triple-tapered titanium stem, J. Arthroplasty 31 (10) (2016) 2231–2236, https://doi.org/10.1016/j.arth.2016.04.037.
[44] X.Y. Ma, Y.F. Feng, Z.S. Ma, X. Li, J. Wang, L. Wang, W. Lei, The promotion of osteointegration under diabetic conditions using chitosan/hydroxyapatite composite coating on porous titanium surfaces, Biomaterials 35 (26) (2014) 7259–7270, https://doi.org/10.1016/j.biomaterials.2014.05.028.
[45] E.M. Lotz, M.B. Berger, Z. Schwartz, B.D. Boyan, Regulation of osteoclasts by osteoblast lineage cells depends on titanium implant surface properties, Acta Biomater. (2017), https://doi.org/10.1016/j.actbio.2017.12.039.
[46] K. Kapat, P.K. Srivas, A.P. Rameshbabu, P.P. Maity, S. Jana, J. Dutta, P. Majumdar, D. Chakrabarti, S. Dhara, Influence of porosity and pore-size distribution in Ti6Al4V foam on physicomechanical properties, osteogenesis, and quantitative validation of bone ingrowth by micro-computed tomography, ACS Appl. Mater. Interfaces 9 (45) (2017) 39235–39248, https://doi.org/10.1021/acsami.7b13960.
[47] P. Xiu, Z. Jia, J. Lv, C. Yin, Y. Cheng, K. Zhang, C. Song, H. Leng, Y. Zheng, H. Cai, Z. Liu, Tailored surface treatment of 3D printed porous Ti6Al4V by microarc oxidation for enhanced osseointegration via optimized bone in-growth patterns and interlocked bone/implant interface, ACS Appl. Mater. Interfaces 8 (28) (2016) 17964–17975, https://doi.org/10.1021/acsami.6b05893.
[48] S. Bose, S. Tarafder, A. Bandyopadhyay, Effect of chemistry on osteogenesis and angiogenesis towards bone tissue engineering using 3D printed scaffolds, Ann. Biomed. Eng. 45 (1) (2017) 261–272, https://doi.org/10.1007/s10439-016-1646-y.
[49] N. Zhao, D. Zhu, Endothelial responses of magnesium and other alloying elements in magnesium-based stent materials, Metall 7 (1) (2015) 118–128, https://doi.org/10.1039/c4mt00244j.
[50] J. Walker, S. Shadanbaz, T.B. Woodfield, M.P. Staiger, G.J. Dias, Magnesium biomaterials for orthopedic application: a review from a biological perspective, J. Biomed. Mater. Res. B Appl. Biomater. 102 (6) (2014) 1316–1331, https://doi.org/10.1002/jbm.b.33113.
[51] M. Nabiyouni, T. Bruckner, H. Zhou, U. Gbureck, S.B. Bhaduri, Magnesium-based bioceramics in orthopedic applications, Acta Biomater. 66 (2018) 23–43, https://doi.org/10.1016/j.actbio.2017.11.033.
[52] K. Kusnierczyk, M. Basista, Recent advances in research on magnesium alloys and magnesium-calcium phosphate composites as biodegradable implant materials, J. Biomater. Appl. (2016), https://doi.org/10.1177/0885328216657271.
[53] Y. Chen, Z. Xu, C. Smith, J. Sankar, Recent advances on the development of magnesium alloys for biodegradable implants, Acta Biomater. 10 (11) (2014) 4561–4573, https://doi.org/10.1016/j.actbio.2014.07.005.
[54] M. Pogorielov, E. Husak, A. Solodivnik, S. Zhdanov, Magnesium-based biodegradable alloys: degradation, application, and alloying elements, Interv Med Appl Sci 9 (1) (2017) 27–38, https://doi.org/10.1556/1646.9.2017.1.04.
[55] A.H. Martinez Sanchez, B.J. Luthringer, F. Feyerabend, R. Willumeit, Mg and Mg alloys: how comparable are in vitro and in vivo corrosion rates? A review, Acta Biomater. 13 (2015) 16–31, https://doi.org/10.1016/j.actbio.2014.11.048.
[56] X. Li, X. Liu, S. Wu, K.W.K. Yeung, Y. Zheng, P.K. Chu, Design of magnesium alloys with controllable degradation for biomedical implants: from bulk to surface, Acta Biomater. 45 (2016) 2–30, https://doi.org/10.1016/j.actbio.2016.09.005.
[57] N.T. Kirkland, N. Birbilis, M.P. Staiger, Assessing the corrosion of biodegradable magnesium implants: a critical review of current methodologies and their limitations, Acta Biomater. 8 (3) (2012) 925–936, https://doi.org/10.1016/j.actbio.2011.11.014.
[58] D.O. Costa, P.D. Prowse, T. Chrones, S.M. Sims, D.W. Hamilton, A.S. Rizkalla, S.J. Dixon, The differential regulation of osteoblast and osteoclast activity by surface topography of hydroxyapatite coatings, Biomaterials 34 (30) (2013) 7215–7226, https://doi.org/10.1016/j.biomaterials.2013.06.014.
[59] H.R. Kang, C.J. da Costa Fernandes, R.A. da Silva, V.R.L. Constantino, I.H.J. Koh, W.F. Zambuzzi, Mg-Al and Zn-Al layered double hydroxides promote dynamic expression of marker genes in osteogenic differentiation by modulating mitogen-activated protein kinases, Adv Healthc Mater (2017), https://doi.org/10.1002/adhm.201700693.
[60] L. Zhang, J. Pei, H. Wang, Y. Shi, J. Niu, F. Yuan, H. Huang, H. Zhang, G. Yuan, Facile preparation of poly(lactic acid)/brushite bilayer coating on biodegradable magnesium alloys with multiple functionalities for orthopedic application, ACS Appl. Mater. Interfaces 9 (11) (2017) 9437–9448, https://doi.org/10.1021/acsami.7b00209.
[61] D. Zou, Z. Zhang, J. He, S. Zhu, S. Wang, W. Zhang, J. Zhou, Y. Xu, Y. Huang, Y. Wang, W. Han, Y. Zhou, S. Wang, S. You, X. Jiang, Y. Huang, Repairing critical-sized calvarial defects with BMSCs modified by a constitutively active form of hypoxia-inducible factor-1alpha and a phosphate cement scaffold, Biomaterials 32 (36) (2011) 9707–9718, https://doi.org/10.1016/j.biomaterials.2011.09.005.
[62] S. Yoshizawa, A. Brown, A. Barchowsky, C. Sfeir, Magnesium ion stimulation of bone marrow stromal cells enhances osteogenic activity, simulating the effect of magnesium alloy degradation, Acta Biomater. 10 (6) (2014) 2834–2842, https://doi.org/10.1016/j.actbio.2014.02.002.
[63] C.Y. Huang, Y.L. Hsieh, D.T. Ju, C.C. Lin, C.H. Kuo, Y.F. Liou, T.J. Ho, C.H. Tsai, F.J. Tsai, J.Y. Lin, Attenuation of magnesium sulfate on CoCl(2)-induced cell death by activating ERK1/2/MAPK and inhibiting HIF-1alpha via mitochondrial apoptotic signaling suppression in a neuronal cell line, Chin. J. Physiol. 58 (4) (2015) 244–253, https://doi.org/10.4077/CJP.2015.BAD296.
[64] J.H. de Baaij, J.G. Hoenderop, R.J. Bindels, Magnesium in man: implications for health and disease, Physiol. Rev. 95 (1) (2015) 1–46, https://doi.org/10.1152/physrev.00012.2014.